Molecular magnetic properties and properties of magnetically induced current densities

A Thesis

submitted to
Indian Institute of Science Education and Research Pune
in partial fulfillment of the requirements for the
BS-MS Dual Degree Programme

by

Rahul Kumar Jinger

Indian Institute of Science Education and Research Pune
Dr. Homi Bhabha Road,
Pashan, Pune 411008, INDIA.

April, 2020

Supervisors: Prof. Dage Sundholm and Maria Dimitrova

© Rahul Kumar Jinger 2020

All rights reserved

Certificate

This is to certify that this dissertation entitled Molecular magnetic properties and properties of magnetically induced current densities towards the partial fulfilment of the BS-MS dual degree programme at the Indian Institute of Science Education and Research, Pune represents study/work carried out by Rahul Kumar Jinger at the Department of Chemistry, University of Helsinki under the supervision of Prof. Dage Sundholm and Maria Dimitrova, Department of Chemistry, University of Helsinki, Finland during the academic year 2019–2020.

Sundholm,
Dage M B

Digitally signed by Sundholm,
Dage M B
Date: 2020.05.30 15:56:21
+03'00'

Prof. Dage Sundholm

Rahul Kumar Jinger

Committee:

Dage Sundholm

Anirban Hazra

This thesis is dedicated to my sister for always being there for me

Declaration

I hereby declare that the matter embodied in the report entitled Molecular magnetic properties and properties of magnetically induced current densities are the results of the work carried out by me at the Department of Chemistry, University of Helsinki, Finland under the supervision of Prof. Dage Sundholm and Maria Dimitrova and the same has not been submitted elsewhere for any other degree.

Sundholm,
Dage M B

Digitally signed by
Sundholm, Dage M B
Date: 2020.05.30 15:55:46
+03'00'

Prof. Dage Sundholm

Rahul Kumar Jinger

Acknowledgments

Firstly, I would like to express my sincere gratitude to my supervisor Prof. Dage Sundholm for the continuous support of my Master thesis and related research, for his patience, motivation, and immense knowledge. His guidance helped me in all the time of research and writing of this thesis.

Besides my advisor, I would like to thank thesis advisory committee member: Prof. Anirban Hazra for his insightful comments and encouragement, but also for the hard questions which motivated me to widen my research from various perspectives.

I would like to thank my fellow labmates and friends Maria Dimitrova and Lukas Wriz and the rest of the members of group for the friendly atmosphere during my stay there.

I thank Prof. Dage Sundholm and Maria Dimitrova for their constant help, guidance and all the suggestions regarding the writing of this thesis and the project.

I thank all my friends without whom this Master Thesis could have never been such a great experience, no words form me are enough to thank them.

Lastly and most importantly I would like to thank my family: my parents and my sister for always supporting me throughout the thesis and in my life in general.

Abstract

This thesis project aims to study magnetic properties and current densities of molecules exposed to magnetic fields using the fully numerical Gauge Including Magnetically Induced Currents (GIMIC) [1] method that has been developed by the Helsinki group and their collaborators. The magnetically induced current density has been studied for molecules like benzene and cyclopentadienyl anion, which are aromatic and cyclobutadiene, which is antiaromatic. Ring-current pathways have been calculated for caffeine by numerically integrating the strength of the current density flowing through-plane intersecting chemical bonds of the molecular rings. The current densities of two isomers of cyclic $C_2B_2NH_5$ have also been investigated. The paratropic and diatropic contributions to the current densities were identified and separated using a novel computational method developed in Helsinki. A method for analyzing spatial contributions to the nuclear magnetic shielding has been developed and applied to benzene as a test case. The approach has been used in studies on CH_4, CF_4, $CH_3{}^-$ and $CF_3{}^-$.

Contents

Abstract **xi**

List of Figures **1**

List of Tables **3**

1 Introduction **5**

2 The molecular energy **9**

3 Molecular electronic structure methods **13**

3.1 The mean-field approximation 13

3.2 Perturbation theory 15

3.3 Density functional theory 16

4 Molecular response to a magnetic field **19**

4.1 The magnetically induced current density 20

4.2 Analytic-derivative-based current-density theory 21

5 Computational details **25**

5.1 Tropicity detection 26

5.2 The current density and tropicity 28
5.3 Calculation of the strength of the current density 29
5.4 Visualisation of shielding constants in space 30

6 Results and discussion **35**

List of Figures

5.1 Magnitude of the current densities in (a) benzene, (b) cyclobutadiene 29

5.2 Integration plane cutting the bond 30

5.3 Spatial contribution to the isotropic magnetic shielding of points in space for (a) carbon (b) hydrogen of benzene. 33

5.4 Spatial contribution to the isotropic magnetic shielding of points in space for (a) carbon (b) hydrogen of benzene in higher resolution 33

5.5 Spatial contribution to the isotropic magnetic shielding of points in space for (a) boron (b) nitrogen (c) carbon of NBBCC 34

6.1 Strength of the ring currents in benzene, cyclobutadiene, and the cyclopentadienyl anion obtained by integrating through a C−C bond starting from the centre of the molecular ring to 8 a_0 away from the bond. 37

6.2 Strength of the ring currents in benzene, cyclobutadiene, and the cyclopentadienyl anion obtained by integrating through a C atom starting from the centre of the molecular ring to 8 a_0 away from the atom. 38

6.3 Magnitude of current density in the cyclopentadienyl anion 39

6.4 Magnitude of current density in naphthalene 39

6.5 Strength of the ring currents in napthalene obtained by integrating through a C−C bond and C atom starting from the centre of the molecular ring to 8 bohr away 40

6.6 Magnitude of the current densities in (a) NBBCC and (b) NB_2CBH_5 molecules 41

6.7 Strength of currents in (a)NBBCC and (b) NBCCB molecules along the C−C bond 41

6.8 Magnitude of current density in caffeine 42

6.9 Strength of currents in (a) five-membered ring (b) six-membered ring in caffeine 42

6.10 Spatial contribution to the isotropic magnetic shielding constant of the carbon atom in (a) CF_3^- (b) CH_3^- along a C−X bond (X= F or H) 44

6.11 Spatial contribution to the isotropic magnetic shielding constant for 'X' in (a) CF_4 (b) CH_4 along the X−C−X plane (X= F or H) 44

6.12 Spatial contribution to the isotropic magnetic shielding constant of the carbon atom in (a) CF_4 (b) CH_4 along a X-C-X plane (X= F or H) 45

6.13 Spatial contribution to the isotropic magnetic shielding constant for 'X' in (a) CF_3^- (b) CH_3^- along the C-X bond (X= F or H) 45

List of Tables

6.1 *The isotropic magnetic shielding constants of C and H of benzene as obtained by* GIMIC *and* TURBOMOLE . . . 35

6.2 *Paratropic and diatropic contributions to the shielding constant* . . . 36

6.3 *Contributions to the shielding constant with a grid spacing of 0.03* a_0 . . . 36

6.4 *Current strengths (in nA* T^{-1}*) of the diatropic and paratropic contributions to the ring current of benzene and cyclobutadiene* . . . 38

6.5 *Current strengths (in nA* T^{-1}*) for the five-membered rings with two boron atoms, two carbon atoms and one nitrogen atom obtained by integrating through a chemical bond.* . . . 40

6.6 *The calculated isotropic magnetic shielding constants of* CF_3^-, CH_3^-, CF_4 *and* CH_4 . . . 43

6.7 *The isotropic magnetic shielding decomposed into paratropic and diatropic contributions* . . . 43

Chapter 1

Introduction

When a molecule is placed in an external magnetic field, its electrons interact with the magnetic field and the angular momentum operator couples, as a result of which, they start precessing around the atoms and throughout the molecule. This electronic motion gives rise to a magnetically induced current density along the molecule. According to Faraday's law, the induced current density in most molecules induces a secondary magnetic field that opposes the direction of the external magnetic field.

The effect of the external magnetic field is quite similar to the effect of magnetic fields on a ring in classical physics. For molecules, however, quantum effects must also be taken into account as spatially separated magnetically induced currents might flow in either the classical or the non-classical direction. The classical current effectively weakens the field while the non-classical currents enhance the magnetic field. The currents flowing in the classical and non-classical directions are called diatropic and paratropic currents, respectively.

Current density

Magnetic interactions are generally quite weak compared to electrostatic forces in the molecule, and hence most quantum mechanical approaches to understand these interactions use perturbation theory. At the perturbation theory level, the magnetic field is assumed to be weak and time-independent, and the current density is the first-order response to the applied magnetic field.

Knowledge about the current density is relevant because the current density is a map of how the electron moves in the molecular systems upon exposure to external magnetic fields. However, it is still not possible to obtain this information using experimental methods, and hence theoretical calculations are mandatory in understanding them. Quantities like the nuclear magnetic resonance (NMR) chemical shifts and magnetic susceptibilities can be related to the magnetically induced current density via Biot–Savart law [2].

The magnetic shielding is a rank-2 tensor that describes the relative change in the local magnetic field at the nuclear position relative to the external magnetic field. This change in the local magnetic field arises from the interaction of the electron cloud with the external field and can lead to shielding of the nucleus where the local magnetic field is increased with respect to the external field or de-shielding where the local magnetic field is decreased. In general, shielding is thought to arise from a spherical charge density, while de-shielding arises from non-spherical charge density originating from electrons in p- or higher angular momentum orbitals [3].

In NMR spectroscopy, the measured property is the chemical shift as a function of the resonance frequency of the nucleus relative to a given standard. The formal relation between the chemical shift and shielding tensors is given as

$$\delta = \mathbf{1}\sigma_{\mathrm{iso}} - \sigma, \tag{1.1}$$

where δ is the chemical shift tensor, σ is the shielding tensor, $\mathbf{1}$ is the unitary matrix and σ_{iso} is the trace of the shielding tensor and is known as the isotropic shielding of the standard reference used in the NMR experiments.

However, determining the σ_{iso} is quite difficult as it involved the determination of the paramagnetic contributions to the shielding using its relationship with the spin rotational constant and the corresponding diamagnetic contribution using quantum mechanical methods [4]. The formal definition of the components of the shielding tensor is:

$$\sigma_{\alpha\beta} = \frac{\partial^2 E}{\partial m_{I_\alpha} \partial B_\beta}, \tag{1.2}$$

where E is the total electronic energy of the molecule, B is the external magnetic field, and

m^I is the magnetic moment of the nucleus of interest. From this equation, we can conclude that the shielding tensor is an anti-symmetric tensor because exchanging the indices α and β leads to a different quantity, *i.e.* $\sigma_{\alpha\beta} \neq \sigma_{\beta\alpha}$.

$$\sigma_{\alpha\beta} = \frac{\partial^2 E}{\partial m_{I_\alpha} \partial B_\beta} \neq \frac{\partial^2 E}{\partial m_{I_\beta} \partial B_\alpha} = \sigma_{\beta\alpha}. \tag{1.3}$$

Aromaticity

The concept of aromaticity lies at the very heart of chemistry. In modern textbooks of organic chemistry, aromatic molecules are described as having pronounced stability, planar geometry, energetics, and magnetic properties. However, from the beginning of its conception, the notion of aromaticity turned out to be controversial, difficult to understand, and to convey in a few words.

According to the ring-current model, magnetically induced current density vortices arise when a molecule is placed in an external magnetic field [2]. The current density reflects the electronic structure of the molecule giving a unique representation of its properties. Molecules that sustain a non-zero net current strength exhibit aromatic or anti-aromatic properties depending on the direction of the current flow with respect to the external magnetic field. A typical feature of aromatic molecules is the presence of conjugated π-electron pathways along the molecular ring. Aromaticity can be reliability studied using the ring-current criterion [2]. Although traditionally associated with the stability and chemical properties of molecules, the abstract concept of aromaticity is of great importance and goes beyond chemical reactivity. The highly delocalized excited state usually makes the molecules suitable as semi-conductors and chromophores, which are of practical interest.

The goal of the thesis was to understand the theory behind the current density and shielding tensor and to obtain a visual representation for them. The currents in the molecules can be separated into diatropic and paratropic using the tropicity detection algorithm developed in the group.

The work in this thesis is structured as follows. The following chapter presents the time-independent Schrödinger equation and leads us to the expression for molecular energy in terms of the one- and two- electrons integrals. Chapter 3 discusses some of the commonly used approximation methods to calculate the wavefunction and the total energy of the molecular system. Chapters 4 and 5 introduce the underlying theory behind the GIMIC method and the tropicity detection program. Chapter 4 focuses on obtaining an expression for the current density, while Chapter 5 introduces the methods used to study the current density, the tropicity detection algorithm, and the expression for magnetic shielding tensor for the molecules.

Chapter 2

The molecular energy

The time-independent Schrödinger equation can be written as $\hat{H}\Psi = E\Psi$, where $\hat{H}$ is the Hamiltonian and Ψ is the wave function [5–8]. In atomic units, the molecular Hamiltonian is expressed as

$$\hat{H} = -\frac{1}{2}\sum_{i}^{N}\nabla_i^2 + \sum_{i>j}^{N}\frac{1}{r_{ij}} - \sum_{a}^{k}\sum_{i}^{N}\frac{Z_a}{r_{ai}} - \sum_{a}^{k}\frac{1}{2m_a}\nabla_a^2 + \sum_{a>b}^{k}\frac{Z_aZ_a}{R_{ab}}, \tag{2.1}$$

where N is the number of the electrons, k is the number of nuclei, m_i is the mass of the i^{th} nucleus, Z_a is the charge on a^{th} nucleus and the operator r_{ij} is the distance between electrons i and j. Using the Born-Oppenheimer approximation [9], the nuclear degrees of freedom and the electronic degrees of freedom can be separated, which makes the wave function only parametrically dependent on the nuclear coordinates. The wave function then depends on $4N$ variables, including the electron spin.

The electronic wave function should be consistent with the Born probability interpretation [10] *i.e.*,

$$\int d\mathrm{x}_1 \ldots d\mathrm{x}_N \Psi(\mathrm{x}_1 \ldots \mathrm{x}_N)^* \psi(\mathrm{x}_1 \ldots \mathrm{x}_N) = 1, \tag{2.2}$$

where Ψ^* is the complex conjugate and $\mathrm{x} = (r_1, r_2, r_3, \sigma)$, with $\sigma \in \{\alpha, \beta\}$ is the electron spin.

For a closed-shell system, $i.e$ molecules with no unpaired electrons, the spin can be separated from the spatial dimensions and integrated separately, leaving $3N$ degrees of freedom per electron. The electron density of the system is then

$$\rho(\mathrm{r}) = N \int \mathrm{r}_2 \ldots d\mathrm{r}_N \Psi(\mathrm{r}, \mathrm{r}_2, \ldots \mathrm{r}_N)^* \Psi(\mathrm{r}, \mathrm{r}_2, \ldots \mathrm{r}_N). \tag{2.3}$$

To solve the Schrödinger equation, we expand the wavefunction in a basis of $3N$-dimensional functions called Slater determinants given as $\Phi = \det|\phi_p(\mathrm{r}_1) \ldots \phi_q(\mathrm{r}_N)|$. The one-particle functions can be then written as a linear combination of atom-centred functions optimised to resemble the atomic orbitals,

$$\phi_a(\mathrm{r}) = \sum_{\mu}^{N_{AO}} C_{\mu a} \chi_\mu(\mathrm{r}). \tag{2.4}$$

The atomic orbitals (AO) are constructed using the Gaussian Type Orbitals (GTOs) given as

$$\chi_\mu(\mathrm{r}) = \sum_{\xi} w_{\xi\mu} r_x^{l_x} r_y^{l_y} r_z^{l_z} e^{-\alpha_{\xi\mu} \mathrm{r}^2}, \tag{2.5}$$

where $\alpha_{\xi\mu}$ are the orbital exponents, $w_{\xi\mu}$ are the contraction coefficients and $\{l_{\{x,y,z\}} \in Z_+\}$ are the pre-factor components related to the orbital angular momentum. The principal reason for using GTOs is due to their locality and the "Gaussian Product Theorem", which guarantees that the product of two GTOs centred on two different atoms can be expressed as a finite sum of Gaussian centred on a point along the axis joining the two points. A function of two variables can be expanded by considering the expansion coefficients as functions of the second variable. This function can again be expanded in the same basis

$$\Phi(\mathrm{r}_1, \mathrm{r}_2) = \sum_{\mu} C_\mu(\mathrm{r}_2) \chi_\mu(\mathrm{r}_1) = \sum_{\mu\nu} C_{\mu\nu} \chi_\mu(\mathrm{r}_1) \chi_\nu(\mathrm{r}_2). \tag{2.6}$$

Hence the exact N-particle wave function can be written as

$$\Psi = \sum_k c_k \sum_{n=1}^{N!} (-1)^{p_n} \mathcal{P}_n \prod_i^N \phi_i^{\{k\}}(\mathrm{r}_i) \tag{2.7}$$

where k is the k^{th} set of MOs. The permutation operator, $\mathcal{P}_n$ ensures fermionic antisymmetry of the wave function by generating the n^{th} permutation of the electronic coordinates r_i and p_n is the number of transpositions needed to generate the permutation.

A very elegant way of constructing a wave function of the proper symmetry, is through the formalism of second quantization. Second quantization revolves around a set of abstract creation and annihilation operators acting on Slater determinants. An electron is created in a spin-orbital ϕ_p from the vacuum by the *creation operator* $a_p^\dagger \left|\phi_q\phi_r\right\rangle = \left|\phi_p\phi_q\phi_r\right\rangle$. The conjugate operator is called the *annihilation operator*, $a_p \left|\phi_p\phi_q\phi_r\right\rangle = \left|\phi_q\phi_r\right\rangle$ $(p \neq q, r)$ which destroys the electron in a spin-orbital ϕ_p. The following anti-commutation relations exists for the two operators

$$\left.\begin{aligned} \{a_p^\dagger, a_q^\dagger\} &= a_p^\dagger a_q^\dagger + a_q^\dagger a_p^\dagger = 0 \\ \{a_p, a_q\} &= a_p a_q + a_q a_p = 0 \\ \{a_p, a_q^\dagger\} &= a_p a_q^\dagger + a_q^\dagger a_p = \delta_{pq} \end{aligned}\right\} \Rightarrow \begin{aligned} a_p^\dagger a_q^\dagger &= -a_q^\dagger a_p^\dagger \\ a_p a_q &= -a_q a_p \\ a_p a_q^\dagger &= \delta_{pq} - a_q^\dagger a_p \end{aligned} \quad . \tag{2.8}$$

Using the formalism of the *creation* and *annihilation* operators, the electronic Hamiltonian can be written as

$$\hat{H} = \sum_{pq} h_{pq} a_p^\dagger a_q + \frac{1}{4} \sum_{pqrs} g_{pqrs} a_p^\dagger a_q^\dagger a_s a_r, \tag{2.9}$$

where h_{pq} and g_{pqrs} are given as

$$h_{pq} = \left\langle \phi_p(1) \right| \hat{h} \left| \phi_q(1) \right\rangle \quad \text{with} \quad \hat{h} = -\frac{1}{2}\nabla^2(1) - \sum_A^K \frac{Z_A}{r_{1A}} \tag{2.10}$$

$$g_{pqrs} = \left\langle \phi_p(1)\phi_q(2) \right| r_{12}^{-1} \left| \phi_r(1)\phi_s(2) \right\rangle - \left\langle \phi_p(1)\phi_q(2) \right| r_{12}^{-1} \left| \phi_s(1)\phi_r(2) \right\rangle = \left\langle pq \right| \left| rs \right\rangle . \tag{2.11}$$

Using the anti-commutation relations, the energy expression can be reduced to involve only specific integrals and orbital coefficients. The electronic energy can thus be written in matrix form as

$$E = \sum_{\mu\nu} h_{\mu\nu} D_{\mu\nu} + \frac{1}{2} \sum_{\mu\nu\sigma\rho} g_{\mu\sigma\nu\rho} d_{\mu\sigma\nu\rho}, \tag{2.12}$$

where $D_{\mu\nu}$ and $d_{\mu\sigma\nu\rho}$ are the one- and two-electron density matrices, $h_{\mu\nu}$ and $g_{\mu\sigma\nu\rho}$ are the one- and two- electron interaction integrals respectively and are given as

$$h_{\mu\nu} = \langle \chi_\mu | \hat{h} | \chi_\nu \rangle \quad \text{and} \quad g_{\mu\sigma\nu\rho} = \langle \chi_\mu \chi_\sigma | \chi_\nu \chi_\rho \rangle \,, \tag{2.13}$$

Chapter 3

Molecular electronic structure methods

3.1 The mean-field approximation

The Hartree-Fock (HF) approximation [11–13] is the computationally least demanding *ab initio* wave function based method for calculating the molecular energy. In the HF approximation, the wave function is truncated at the first term in the expansion of Eq. 2.7 *i.e.*, wave function of the system can be approximated by a single Slater determinant.

The energy of the one-determinant trial function is

$$\begin{aligned} E[\Phi] = \langle\Phi|\,\hat{H}\,|\Phi\rangle = \sum_i \langle\phi_i|\,\hat{h}\,|\phi_i\rangle + \frac{1}{2}\sum_{ij}\big(\langle\phi_i\phi_j|\,r_{12}^{-1}|\,|\phi_i\phi_j\rangle - \langle\phi_i\phi_j|\,r_{12}^{-1}\,|\phi_j\phi_i\rangle\big) \\ = \sum_i \langle\phi_i|\,\hat{h}\,|\phi_i\rangle + \frac{1}{2}\sum_{ij}\langle\phi_i|\,(J_j - K_j)\,|\phi_i\rangle\,, \end{aligned} \tag{3.1}$$

where J describes the interaction between two charge distributions and is called the Coulomb operator, and K arises from the antisymmetry of the wave function and is called the exchange operator. Linear variations under the constraint that the one-particle functions remain orthonormal on the trial functions gives the Hartree-Fock equations,

$$f\phi_i = \epsilon_i\phi_i, \tag{3.2}$$

where f is the Fock operator given as [14]

$$f(1) = \hat{h}(1) + \sum_i (J_i(1) - K_i(1)) = h(1) + v^{\mathrm{HF}}(1). \tag{3.3}$$

Solving the HF equations, yields the molecular orbitals ϕ_i and the orbital energies ϵ_i. However, due to the variational principle [15], the obtained energies are always higher than the ground state energy. The equations must be solved iteratively until self consistency is reached.

The eigenvalue of the total Fock operator, $F = \sum_i f(i)$ is

$$F\left|\Psi_0^{\mathrm{HF}}\right\rangle = E_0\left|\Psi_0^{\mathrm{HF}}\right\rangle, \tag{3.4}$$

where $E_0 = \sum_i^N \epsilon_i$. This eigenvalue is not the real ground state energy due to double counting of the electron-electron interactions. The true HF ground state energy is

$$E_{\mathrm{HF}} = \left\langle\Psi_0^{\mathrm{HF}}\right| \hat{H} \left|\Psi_0^{\mathrm{HF}}\right\rangle = \sum_i^N \epsilon_i - \frac{1}{2}\sum_{ij}^N \langle\phi_i|\left(J_j - K_j\right)|\phi_i\rangle, \tag{3.5}$$

which is not an eigenvalue of the Fock operator. The difference between the mean-field energy and the exact energy is due to the fact that electrons do not move independently of each other, which is called the correlation energy. Electron correlation lowers the probability of two electrons being close to each other and lowers the overall energy by reducing the electron-electron repulsion.

3.2 Perturbation theory

In quantum mechanics, perturbation theory [16] is an approximation scheme for describing a complicated quantum system in terms of a simpler one. The idea is to start with a simple system for which a mathematical solution is known, and add a "perturbing" Hamiltonian representing a weak disturbance to the system. Suppose the eigenvalues of a Hamiltonian H_0 is known, and we want to know the energy of the Hamiltonian $H = H_0 + \lambda H_1$, where $\{\lambda \in [0,1]\}$ is a parameter. When the effects of H_1 on the energy are small compared to H_0, the eigenvalues and eigenfunctions of H can be found by expanding both the energy and wave function in a Taylor series in λ with

$$\begin{aligned}(H_0 + \lambda H_1)(\Psi_n^{(0)} + \lambda \Psi_n^{(1)} + \lambda^2 \Psi_n^{(2)} + \ldots) = \\ (E_n^{(0)} + \lambda E_n^{(1)} + \lambda^2 E_n^{(2)} + \ldots)(\Psi_n^{(0)} + \lambda \Psi_n^{(1)} + \lambda^2 \Psi_n^{(2)} + \ldots),\end{aligned} \tag{3.6}$$

where

$$E_n^{(0)} = \left\langle \Psi_n^{(0)} \right| H_0 \left| \Psi_n^{(0)} \right\rangle \quad \text{and} \quad E_n^{(k)} = \left\langle \Psi_n^{(0)} \right| H_1 \left| \Psi_n^{(k-1)} \right\rangle . \tag{3.7}$$

Using the complete set of eigenfunctions of the unperturbed Hamiltonian, the perturbed wave function can be expanded as

$$\Psi_n^{(k)} = \sum_i c_{ni}^{(k)} \Psi_i^{(0)}. \tag{3.8}$$

The first-order energy correction can be calculated simply as the expectation value of the unperturbed zero-order wave function. The expansion coefficients for the first-order correction to the wave function can be calculated as,

$$c_{ni}^{(1)} = \frac{\left\langle \Psi_n^{(0)} \right| H_1 \left| \Psi_i^{(0)} \right\rangle}{E_n^{(0)} - E_i^{(0)}}. \tag{3.9}$$

The second-order energy correction is then

$$E_n^{(2)} = \sum_{i \neq n} \frac{\left\langle \Psi_n^{(0)} \middle| H_1 \middle| \Psi_i^{(0)} \right\rangle \left\langle \Psi_i^{(0)} \middle| H_1 \middle| \Psi_n^{(0)} \right\rangle}{E_n^{(0)} - E_i^{(0)}}. \tag{3.10}$$

3.3 Density functional theory

Density functional theory (DFT) is a quantum-mechanical method that describes the properties of many-body systems by using functionals, *i.e.*, functions of another function, which in this case is the electron density. Thus, instead of having to work with a $3N$-dimensional wave function, every molecular ground-state property can be calculated from a quantity which is only 3-dimensional. However, the exact electron density is not known and is needed to be approximated. In the Kohn-Sham equations [17–19], the density is expanded in a basis of molecular orbitals. The Kohn-Sham energy for a molecular system is

$$E_{\text{KS}} = \langle \hat{h} \rangle + J\{\rho\} + E_{\text{xc}}\{\rho\}, \tag{3.11}$$

where the curly brackets indicate functionals and E_{xc} is the exchange-correlation(XC) functional. The exchange-correlation functional represents the difference between the exact and the approximate systems. It is associated with the Kohn-Sham potential, v_{KS} which is given as

$$v_{\text{KS}}(\mathbf{r}) = v_{ext}(\mathbf{r}) + v_J(r) + v_{\text{xc}}(\mathbf{r}), \tag{3.12}$$

where $v_{\text{ext}}(\mathbf{r})$ is the external potential created by the nuclei, $v_J(r)$ the electrostatic repulsion by the electrons, and $v_{\text{xc}}(\mathbf{r})$ is the exchange-correlation potential.

On substituting the Kohn-Sham potential into the Schrödinger equation, and solving it leads us to the Kohn-Sham equations,

$$\left[-\frac{1}{2}\nabla^2 + v_{\text{KS}}(\mathbf{r})\right]\psi_i(\mathbf{r}) = \epsilon_i\psi_i(\mathbf{r}). \tag{3.13}$$

To apply the Kohn-Sham equations to real molecules, it is necessary to find a good approximation to the exchange-correlation functional which can be done in a lot of different ways. In the local-density approximation (LDA) [20, 21], the electron density is based on the electron gas model by Fermi, Thomas and Dirac. The exchange-correlation energy is calculated by integrating the electron correlation functional scaled by the electron density at each point in space,

$$E_{\mathrm{xc}}^{\mathrm{LDA}} = \int \rho(\mathbf{r})\epsilon(\rho)d^3\mathbf{r}. \tag{3.14}$$

The exchange energy functional in LDA can be solved analytically.

In the generalised-gradient approximation (GGA) [22, 23], the exchange-correlation energy is defined using the derivative of the electron density with respect to the Cartesian coordinates,

$$E_{\mathrm{xc}}^{\mathrm{GGA}} = \int \rho(\mathbf{r})\epsilon(\rho, \nabla\rho)d^3\mathbf{r}. \tag{3.15}$$

The Hartree-Fock method can be considered as an extreme case of DFT with the correlation energy being zero and the exchange energy is exact. This method thus describes the single-determinant problem accurately. The hybrid functionals uses the GGA, LDA as well as a fraction of HF exchange to give approximate results.

$$E_{\mathrm{xc}}^{\mathrm{hybrid}} = E_{\mathrm{xc}}^{\mathrm{LDA}} + a\left(E_{\mathrm{x}}^{\mathrm{HF}} - E_{\mathrm{x}}^{\mathrm{LDA}}\right) + b\delta E_{\mathrm{x}}^{\mathrm{GGA}} + c\delta E_{\mathrm{x}}^{\mathrm{GGA}}\,, \tag{3.16}$$

where a, b and c are parameters. The B3LYP functional is one of the most commonly used hybrid functionals with $a = 0.2$, $b = 0.72$ and $c = 0.81$.

Chapter 4

Molecular response to a magnetic field

As a molecule is exposed to a magnetic field, the electrons in the molecule start precessing due to coupling between their angular momentum and the field. This circular motion in turn induces a current density in the molecule. The current density induces a secondary magnetic field which, in most molecules, opposes the external field, thereby minimizing the effect of the external field. This phenomenon is in many ways similar to classical electrodynamics.

In quantum-mechanical systems however, magnetically induced current densities may also flow in the non-classical direction. The direction of current flow is referred to as *tropicity* and it is defined with respect to the external magnetic field direction. By convention, the current flowing in the classical direction are called diatropic, while the non-classical ones are called paratropic.

The magnetically induced current density describes how electrons move in a system exposed to an external magnetic field. Although the magnetically induced current density is a quantum mechanical observable and an operator for it is defined, there is no equipment available to measure it directly, therefore theoretical calculations must be conducted to study them. Indirect insights on the strength of the current density is obtained from NMR chemical shifts.

4.1 The magnetically induced current density

In presence of a uniform, time-independent magnetic field with a flux B, a current density **J** is induced

$$\mathbf{J}(\vec{\mathrm{r}}) = \frac{i}{2}\int \mathrm{d}\vec{r}_2 ... \mathrm{d}\vec{r}_n (\Psi^*\nabla\Psi - \Psi\nabla\Psi^* + 2i\vec{A}^B\Psi^*\Psi). \tag{4.1}$$

Here, Ψ is the wave function and $\vec{A}^B$ is the vector field describing the external magnetic field,

$$\vec{A}^B(\vec{\mathrm{r}}) = \frac{1}{2}\vec{B} \times (\vec{\mathrm{r}} - \vec{\mathrm{R}}_O), \tag{4.2}$$

in the above equations, $\vec{R}_O$ illustrates the gauge origin of the magnetic field.

For a molecule in a stationary state, the charge-conservation condition becomes $\nabla \cdot \vec{J} = 0$. For a molecules with no unpaired electrons, this reduces to $\vec{J} = 0$ in the absence of an external magnetic field.

For an isotropic medium, the magnetic flux density $\vec{B}$ is uniquely defined by the vector potential $\vec{A}$. However the reverse is not true since

$$\vec{B} = \nabla \times (\vec{A}(\vec{\mathrm{r}}) + \nabla\Phi(\vec{\mathrm{r}})) = \nabla \times \vec{A}(\vec{\mathrm{r}}) \tag{4.3}$$

Here, $\Phi(\vec{\mathrm{r}})$ is an arbitrary scalar function, thus rendering the choice of gauge origin for the magnetic field undermined. The use of finite basis sets inevitably brings gauge dependence in quantum chemical calculations of magnetic properties. In modern calculations of NMR chemical shifts [24] and in calculations of current densities using the GIMIC program, gauge-origin independence is ensured using gauge-including atomic orbitals (GIAOs) given as:

$$\chi_\mu(\mathrm{r}) = e^{-(i/2)(\vec{B}\times\left[\vec{R}_\mu - \vec{R}_O\right]\cdot\vec{r})}\chi_\mu^{(0)}(\vec{r}) \tag{4.4}$$

where ${\chi_\mu}^{(0)}(r)$ denotes a standard Gaussian-type basis function with $\vec{R}_\mu$ as the centre.

The vector potentials due to the nuclear magnetic moments of I^{th} nucleus, m_I is given as,

$$\vec{A}^{\vec{m}_I}(\vec{\mathrm{r}}) = \alpha^2 \frac{\vec{m}_I \times (\vec{\mathrm{r}} - \vec{R}_I)}{|\vec{\mathrm{r}} - \vec{R}_I|^3}. \tag{4.5}$$

This vector potential couples with the external magnetic field and the resulting in the total vector potential $\vec{A}$, which contains the terms arising from both the external magnetic field and the nuclear magnetic moment.

$$\vec{A} = \vec{A}^B(\vec{r}) + \sum_{m_I} \vec{A}^{\vec{m}_I}(\vec{\mathrm{r}}) \tag{4.6}$$

4.2 Analytic-derivative-based current-density theory

The electronic energy of a molecule can be written as given in Eq. 2.12 where $h_{\mu\nu}$ and $g_{\mu\nu\sigma\rho}$ are the one- and two-electron interaction integrals given by

$$h_{\mu\nu} = \int d\vec{r} \chi_\mu^* \widehat{h} \chi_\nu \quad \text{and} \quad g_{\mu\nu\sigma\rho} = \int\int d\vec{r}_1 d\vec{r}_2 \chi_\mu^* \chi_\sigma^* r_{12}^{-1} \chi_\nu \chi_\rho \quad , \tag{4.7}$$

$D_{\mu\nu}$ and $d_{\mu\nu\sigma\rho}$ are the one- and two-electron density matrices and $\widehat{h}$ is the one electron Hamiltonian. Differentiating the electronic energy in Eq. 2.12 with respect to the nuclear magnetic moments and the external magnetic field in the limit of zero magnetic field, yields the nuclear magnetic shielding tensor [25–27] given by:

$$\sigma^I_{\alpha\beta} = \frac{\partial^2 E}{\partial m_{I_\alpha} \partial B_\beta}\Big|_{\vec{B}=0, m_I=0} \quad . \tag{4.8}$$

Evaluating Eq. 4.8 together with energy expression in Eq. 2.12 gives the following relation for the magnetic shielding tensor elements:

$$\sigma^I_{\alpha\beta} = \sum_{\mu\nu} D_{\mu\nu} \frac{\partial^2 h_{\mu\nu}}{\partial m_{I_\alpha} \partial B_\beta} + \sum_{\mu\nu} \frac{\partial D_{\mu\nu}}{\partial B_\beta} \frac{\partial h_{\mu\nu}}{\partial m_{I_\alpha}} \quad , \tag{4.9}$$

where $\partial D_{\mu\nu}/\partial B_\beta$ are the magnetically perturbed density matrices in the $\beta = \{x, y, z\}$ Cartesian direction, and $\partial h_{\mu\nu}/\partial m^I_\alpha$ along with $\partial^2 h_{\mu\nu}/\partial m^I_\alpha \partial B_\beta$ as the corresponding derivatives of integrals of $\widehat{h}$.

The interaction energy between the nuclear magnetic moment and the external magnetic field can also be expressed in terms of the current density and the vector potential as [2]:

$$E^{m_I \vec{B}} = -\int \vec{A}^{m_I}(r) \cdot \vec{J}^B(r) d\vec{r} \quad , \tag{4.10}$$

where $\vec{A}^{\vec{m}_I}$ is given in Eq. 4.5.

Using the Eq. 4.10 along with Eq. 2.12, we obtain an alternative expression for the nuclear magnetic shielding,

$$\sigma^I_{\alpha\beta} = -\epsilon_{\alpha\delta\gamma} \int \frac{r_\delta - R_{I\delta}}{|\vec{r} - \vec{R}_I|^3} \mathcal{J}^{B_\beta}_\gamma d\vec{r} \quad , \tag{4.11}$$

where, $\epsilon_{\alpha\delta\gamma}$ is the Levi-Civita symbol, (α, δ, γ) are the Cartesian coordinates, and

$$\mathcal{J}^{B_\beta}_\gamma(r) = \frac{\partial \mathcal{J}_\gamma(r)}{\partial B_\beta}, \tag{4.12}$$

are the matrix elements of the first-order induced current density.

On equating Eq. 4.9 and Eq. 4.12 and introducing the one-electron basis functions, we obtain the relation between the magnetic shielding and the current density matrix [3]. After further simplifying, we obtain the working equation for the calculation of the magnetically induced current density tensor, $\mathcal{J}^{B_\beta}_\gamma(r)$, as:

$$\mathcal{J}_{\alpha}^{B_\beta}(r) = \sum_{\mu\nu} D_{\mu\nu} \frac{\partial \chi_\mu^*(\mathbf{r})}{\partial B_\beta} \frac{\partial h}{\partial m_\alpha^I} \chi_\nu(\mathbf{r}) + \sum_{\mu\nu} D_{\mu\nu} \chi_\mu^*(\mathbf{r}) \frac{\partial h}{\partial m_\alpha^I} \frac{\partial \chi_\nu(\mathbf{r})}{\partial B_\beta}$$
$$+ \sum_{\mu\nu} \frac{\partial D_{\mu\nu}}{\partial B_\beta} \chi_\mu^*(\mathbf{r}) \frac{\partial h}{\partial m_\alpha^I} \chi_\nu(\mathbf{r}) - \epsilon_{\alpha\beta\delta} \big[\sum_{\mu\nu} D_{\mu\nu} \chi_\mu^*(\mathbf{r}) \frac{\partial^2 h}{\partial m_\alpha^I \partial B_\delta} \chi_\nu(\mathbf{r}) \big] \quad (4.13)$$

Since this equation only involves the basis function and derivatives of the basis functions along with the one-electron density matrix, it is easily evaluated at each point in space. The current density tensor is independent of all the nuclear positions as the dependence of each individual contribution on the nuclear position $\vec{R}_I$ cancels out for all the terms.

Implementation

In the GIMIC program, the Eq. 4.13 for $\mathcal{J}_{\alpha}^{B_\beta}(r)$ is implemented in matrix form. The starting point for such a form is a vector $\vec{v}$ whose elements are made up of the basis function values at each grid point. We need to evaluate the derivatives of the basis functions with respect to the 3D coordinates. Due to the field dependence of GIAOs [28, 29], evaluation of the first derivative of the basis functions with respect to components of the external magnetic field as well as a second derivative with respect to the magnetic field B and the 3D coordinates is needed. The expression for the spin contributions to the magnetically induced current density tensor, $\mathcal{J}_{\alpha}^{B_\beta}(r)$ is then given as:

$$\mathcal{J}_{\alpha}^{B_\beta}(r) = \vec{v}^T \mathbf{P}_\beta \vec{d}_\alpha - \vec{b}_\beta^T \mathbf{D} \vec{d}_\alpha + \vec{v}^T \mathbf{D} \vec{q}_{\alpha\beta} - \epsilon_{\alpha\beta\gamma} \frac{1}{2} (\vec{v}^T \mathbf{D} \vec{v}) \vec{r}_\gamma \quad (4.14)$$

where, $\mathbf{D}$ are the atomic orbital (AO) density matrices, $\mathbf{P}_\alpha$ are the corresponding magnetically perturbed AO density matrices and $\vec{b}_\alpha$, $\vec{d}_\alpha$, $\vec{q}_{\alpha\beta}$ are the derivatives of the basis functions and are given as:

$$\mathbf{b}_\alpha = \frac{\partial \vec{v}}{\partial \mathbf{B}_\alpha} \quad , \quad \mathbf{d}_\alpha = \frac{\partial \vec{v}}{\partial \vec{r}_\alpha} \quad , \quad \mathbf{q}_{\alpha\beta} = \frac{\partial^2 \vec{v}}{\partial \vec{r}_\alpha \partial \mathbf{B}_\beta}, \quad (4.15)$$

where the α and β are the Cartesian coordinate axes (x, y, z). The AO perturbed and unperturbed density matrices can be obtained by any standard *an inito* program capable of calculating nuclear magnetic shielding tensors. In this case, the program used was TURBOMOLE [30], the results from which will be presented in the subsequent section.

Chapter 5

Computational details

Nuclear magnetic resonance (NMR) spectroscopy is a spectroscopic technique used to investigate molecular structures. In NMR experiments, the sample is placed in a static magnetic field, which induces magnetic polarization of the nuclear spins in the molecule. The sample is then perturbed with radio waves which are absorbed by the NMR-active nuclei present in the sample. All isotopes that contain an odd number of protons and neutrons, have an intrinsic nuclear magnetic moment and angular momentum *i.e.* a total nonzero nuclear spin.

For a nucleus with spin I and nuclear magnetic moment μ in a magnetic field B_0, the energy level separation is

$$\Delta E = \mu \frac{B_0}{I}. \tag{5.1}$$

The frequency of the electromagnetic radiation that induces a transition between two adjacent energy levels is

$$\nu_0 = \frac{\Delta E}{\hbar}. \tag{5.2}$$

The observed resonant frequencies of the nuclei are heavily dependent on their chemical environment. The electrons around a nucleus generate a small induced magnetic field that generally opposes the applied field B_0. The effective magnetic field B_{eff} is therefore weaker that the applied magnetic field B_0 and depends on the shielding constant [31] for the atom σ,

$$B_{\text{eff}} = B_0 - \sigma B_0 \tag{5.3}$$

5.1 Tropicity detection

In order to determine the contributions from the diatropic and paratropic current density to the nuclear magnetic shielding, the module TROPICITYDETECTION developed in the group was employed. The program classifies whether a given grid point belongs to a diatropic or a paratropic current-density vortex. By repeating the procedure for each grid point, the program can separate diatropic and paratropic contributions to the current density which are then written to different files. The values of current density obtained from GIMIC are only given at discrete grid points which can be adjusted for each calculation. Therefore, the value of current density must be interpolated from the known values at each grid point. To get the value of each point, we use linear interpolation which is based on the 8 closest grid points that form a cuboid around a given point.

In the TROPICITYDETECTION module, trajectories are drawn by extrapolating the current density vector field using the Runge-Kutta method. In the Runge-Kutta method, a function is approximated by adding to an initial value of the function a weighted average of four increments, each of which is a product of the step length (a suitably small constant) and an estimated slope of the function. The function being approximated here is the current density vector field. For a given step length h and a vector $\vec{v}(\vec{a_n})$ at an initial position given by $\vec{a_n}$, the next position is given by

$$\vec{a}_{n+1} = \vec{a}_n + \frac{1}{6}(\vec{k}_1 + 2\vec{k}_2 + 2\vec{k}_3 + \vec{k}_4), \tag{5.4}$$

where

$$\vec{k}_1 = h\vec{v}\left(\vec{a}_n\right), \tag{5.5}$$

$$\vec{k}_2 = h\vec{v}\left(\vec{a}_n + \frac{1}{2}\vec{k}_1\right), \tag{5.6}$$

$$\vec{k}_3 = h\vec{v}\left(\vec{a}_n + \frac{1}{2}\vec{k}_2\right), \tag{5.7}$$

$$\vec{k}_4 = h\vec{v}\left(\vec{a}_n + \frac{1}{2}\vec{k}_3\right). \tag{5.8}$$

An average of these four points are taken such that the increments $\vec{k_1}$ and $\vec{k_2}$ are given more weight as they are based on the slope at the midpoint of the interval. The value of the current density vector field is generally not known at the point $a_n + k$ because the values of the current density are only given at discrete points inside the cube file. Therefore, the value of the current density must be interpolated from the known values. In the TROPICITY-DETECTION program this is done with linear interpolation from the 8 points that form the cuboid which encloses the point a_{n+1} in the cube file. The above process is repeated until the trajectory is completed. However, generally, the exact starting point will not be reached. Approximating the field using linear interpolation and the Runge-Kutta method introduces uncertainties. To circumvent this, the trajectory is extended until a point sufficiently close to the starting point is reached. This can be achieved by checking if the distance between a point and the starting point is less than some fraction of the distance between the starting point and the farthest point from the starting point already included in the trajectory,

$$|\vec{a}_n - \vec{a}_0| < \epsilon\,|\vec{a}_{max} - a_n|\,. \tag{5.9}$$

Setting ϵ to be too large will cause the trajectories to end abruptly and a very small value of ϵ will cause the trajectories to never converge. In the present calculations, the value was selected to be $\epsilon = 0.1$.

Once the trajectory is completed, its tropicity can be determined. For each point $\vec{a}_n$ in the trajectory, the cross product $\vec{v}(\vec{a_n}) \times \vec{v}(\vec{a}_{n+1})$ is taken. The components along $\vec{B}_0$ of these products are then summed,

$$t = \sum_n \vec{B}_0 \left[\vec{v}\left(\vec{a}_n\right) \times \vec{v}(\vec{a}_{n+1}) \right]. \tag{5.10}$$

The parameter t is then used to determine the tropicity of the trajectory. For $t < 0$ we have a paratropic current density, whereas for $t > 0$ we have a diatropic current density.

If the trajectory starting at some point would extend to beyond the cube formed by the grid points, it cannot be completed and the point will not be assigned a tropicity value. This causes some current flux to be ignored when doing calculations, and could be resolved by taking a cube with larger dimensions.

5.2 The current density and tropicity

We have used the PARAVIEW program for visualisation of the current density vector field obtained using GIMIC. A colour scheme is employed to show the strength of the current density where black is the lowest corresponding to a $|J(r)| < 10^{-6}$ nA T^{-1} m^{-2} and increasingly in the order red orange yellow and white which corresponds to a $|J(r)| > 0.1$ nA T^{-1} m^{-2}.

Cross-section of current density reveals the presence of various other smaller domains embedded into the global current density domain. The outermost global current is always diatropic, while in the case of atoms, there is a strong, concentrated current density due to the core electrons. These features are referred to as atomic ring currents [32], and their strength depends on the number of core electrons. Additionally, there are current density vortices present at the chemical bonds, which are called bond currents and are generally weak diatropic currents.

The strongest ring currents are observed when the applied magnetic field is perpendicular to the molecular plane as the p orbitals of the atoms in the conjugated π electron pathway are aligned with the direction of the magnetic field. In polycyclic molecules and non-planar molecules, multiple ring currents can be present. The presence of heteroatoms can alter the ring current pathways depending on the electronegativity of the atom present. For example, in the neighborhood of a nitrogen atom, there are significant local atomic current density domains which enclose the bond currents of the neighboring N$-$H bonds as is visible in the streamline representation of current density in caffeine and a five-membered ring containing

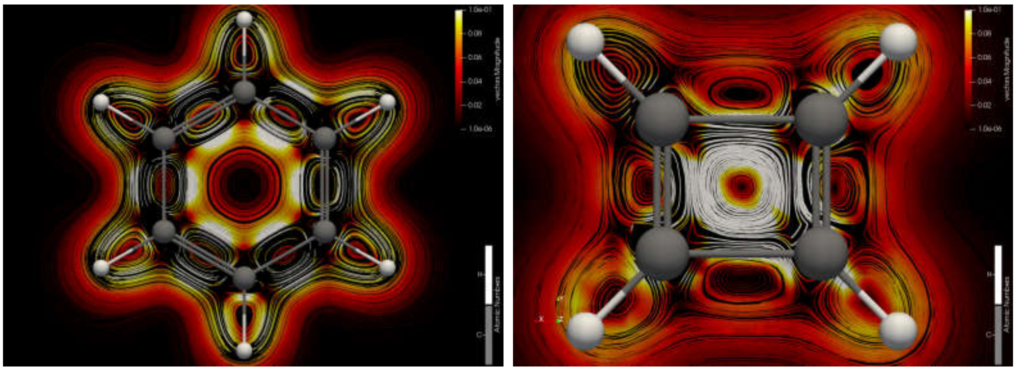

(a) (b)

Figure 5.1: Magnitude of the current densities in (a) benzene, (b) cyclobutadiene

both nitrogen and boron. Heteroatoms cause the formation of complicated patterns of the global ring currents. Ring currents often do not follow planar trajectories, as can be seen for methane and tetrafluoromethane.

5.3 Calculation of the strength of the current density

The strength of current density is calculated by placing an integration plane through a particular current-density domain where the plane is extended from the center of the molecular ring until the current density vanishes along with an 8 a_0 distance above and below so that the whole cross-section of current density domain is evaluated. For each grid point in the plane, we can assign a positive or negative sign depending on the tropicity of the current. However, the tropicty cannot be assigned as tropicity is a global property of the vortex and cannot be characterized by a single point. When a vortex passes through the plane, it first appears to pass in one direction. After crossing the vortex, it appears to come from the opposite direction, due to which the net current vanishes. When the integration plane divides the molecule into two halves, the net current must vanish due to charge conservation.

When the integration plane passes through a bond or an atom vortex, the ring current gets integrated twice as it circles twice the vortex origin. Due to charge conservation, the total ring current strength of a bond or atom vanishes, and hence we can calculate the global net ring-current. The atomic/bond vortex can be seen as a feature in the current strength plot as a peak, which depends on the strength of the atomic vortex. Aromatic molecules

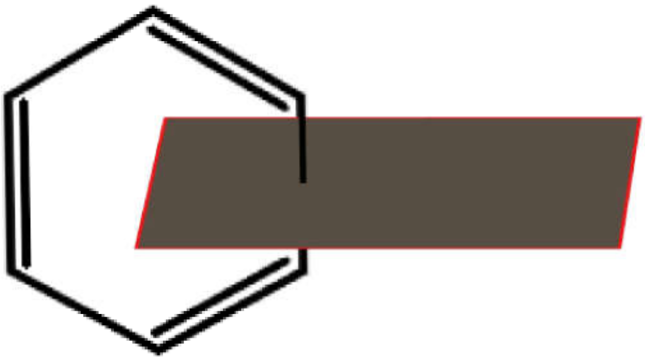

Figure 5.2: Integration plane cutting the bond

generally sustain a positive current strength while anti-aromatic molecules sustain a negative ring current. Molecules with ring-current strengths of ±3 nA T^{-1} are generally considered non-aromatic.

The plane is split vertically into thin slices. Differential contributions to the induced current (in nA $T^{-1}{a_0}^{-1}$) passing through slices of integration plane can be plotted as a function of the z coordinate along the plane. The width of the slice used is 0.005 a_0. The current density is evaluated on the grid 0.002 a_0 apart horizontally.

5.4 Visualisation of shielding constants in space

When a time independent uniform magnetic field acts upon the permanent dipole μ_I of the I^{th} nucleus in a molecule, the resulting perturbing vector potential is

$$A = A^B + A^{m_I}, \tag{5.11}$$

where,

$$A^B = \frac{1}{2}B \times (r - r_0) \quad \text{and} \quad A^{m_I} = \alpha^2 \frac{\mu_I \times \vec{r} - \vec{R}_I}{|\vec{r} - \vec{R}|^3}. \tag{5.12}$$

The electronic wave-function can be expanded as a series to account for the perturbation as

$$\psi = \psi_0 + \psi^B \cdot B + \psi^{m_I} m_I + \ldots, \tag{5.13}$$

where ψ is the ground state wave-function and ψ^B is the electronic wave-function in presence of the magnetic field and is given as

$$|\psi_B\rangle = -\frac{e}{2m_e c\hbar} \sum_{j \neq a} \omega_{ja}^{-1} |j\rangle \langle j| L |a\rangle . \tag{5.14}$$

Since the perturbation from the external magnetic field and the nuclear moments are described by imaginary operators. Hence stationary currents that do not modify the electronic charge distribution are induced.

The first-order current density tensor expanded in a power series is

$$J_\alpha(r) = J_\alpha^{(0)}(r) + \mathcal{J}_\alpha^{B_\beta}(r) B_\beta + \ldots, \tag{5.15}$$

where $\mathcal{J}_\alpha^{B_\beta}(r)$ is the second-rank current density tensor. The second-order interaction energy can be thus be written as [2]

$$W^{BB} = -\frac{1}{2c} \int dV A^B(r) \cdot J^B(r), \tag{5.16}$$

$$W^{m_I B} - \frac{1}{c} \int dV A^{m_I}(r) \cdot J^B(r). \tag{5.17}$$

The magnetic shielding at nucleus I and the magnetic susceptibility are given as

$$\sigma^I_{\alpha\beta} = \frac{\partial^2 W^{m_I B}}{\partial m_{I_\alpha} \partial B_\beta} \quad \text{and} \quad \chi^I_{\alpha\beta} = -\frac{\partial^2 W^{BB}}{\partial B_\alpha \partial B_\beta}, \tag{5.18}$$

and can be written as

$$\sigma^I_{\alpha\delta} = -\frac{1}{c}\epsilon_{\alpha\beta\gamma} \int dV \frac{r_\beta - R_{I\beta}}{|r - R_I|^3} \mathcal{J}^{B_\beta}_\gamma(r), \tag{5.19}$$

$$\chi_{\alpha\delta} = \frac{1}{2c}\epsilon_{\alpha\beta\gamma} \int dV r_\beta \mathcal{J}^{B_\delta}_\gamma(r). \tag{5.20}$$

For any point in space for a particular nucleus, the integrand in Eq. 5.19 is the contribution to the shielding constant of that point to the specific nucleus. The spatial contribution to the carbon and hydrogen nuclei are shown in Fig. 5.3 as well as in Fig. 5.4 in higher resolution.

The second-rank tensor, σ, is expressed as the sum of three tensors of rank 0, 1 and 2 which are the isotropic shielding , the anti-symmetric contribution and the Δ parameter respectively,

$$\sigma = \begin{bmatrix} \sigma_{xx} & \sigma_{xy} & \sigma_{xz} \\ \sigma_{yx} & \sigma_{yy} & \sigma_{yz} \\ \sigma_{zx} & \sigma_{zy} & \sigma_{zz} \end{bmatrix} = \sigma_{\text{iso}} \begin{bmatrix} 1 & 0 & 0 \\ 0 & 1 & 0 \\ 0 & 0 & 1 \end{bmatrix} + \begin{bmatrix} 0 & \sigma^A_{xy} & \sigma^A_{xz} \\ \sigma^A_{yx} & 0 & \sigma^A_{yz} \\ \sigma^A_{zx} & \sigma^A_{zy} & 0 \end{bmatrix} + \begin{bmatrix} \Delta_{xx} & \Delta_{xy} & \Delta_{xz} \\ \Delta_{yx} & \Delta_{yy} & \Delta_{yz} \\ \Delta_{zx} & \Delta_{zy} & \Delta_{zz} \end{bmatrix},$$

where

$$\sigma_{\text{iso}} = \frac{1}{3}(\sigma_{xx} + \sigma_{yy} + \sigma_{zz}), \tag{5.21}$$

$$\sigma^A_{\alpha\beta} = \sigma_{\alpha\beta} - \sigma_{\beta\alpha} \tag{5.22}$$

and

$$\Delta_{\alpha\beta} = \frac{1}{2}(\sigma_{\alpha\beta} + \sigma_{\beta\alpha}) - \sigma_{\text{iso}}\delta_{\alpha\beta}. \tag{5.23}$$

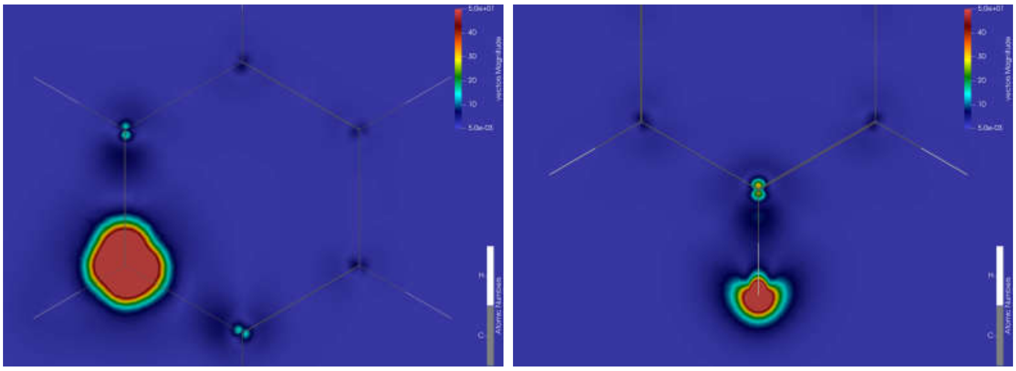

(a) **(b)**

Figure 5.3: Spatial contribution to the isotropic magnetic shielding of points in space for (a) carbon (b) hydrogen of benzene.

As we approach the nucleus, the contribution increases rapidly because of the inverse cubic (r^{-3}) relation with distance. The partial contribution to the isotropic magnetic shielding constant depends on the local environment around the atom. For heteroatoms, the spatial contribution to shielding constant depends on their neighbouring atoms and their electronegativity which can be seen in Fig 5.5.

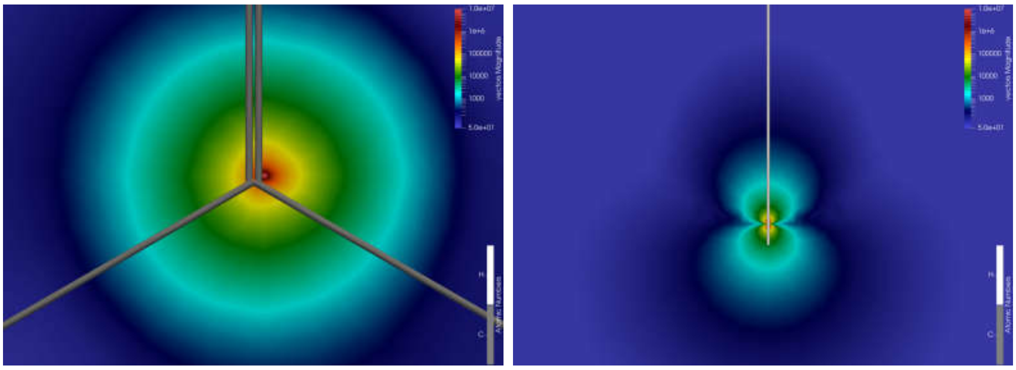

(a) **(b)**

Figure 5.4: Spatial contribution to the isotropic magnetic shielding of points in space for (a) carbon (b) hydrogen of benzene in higher resolution

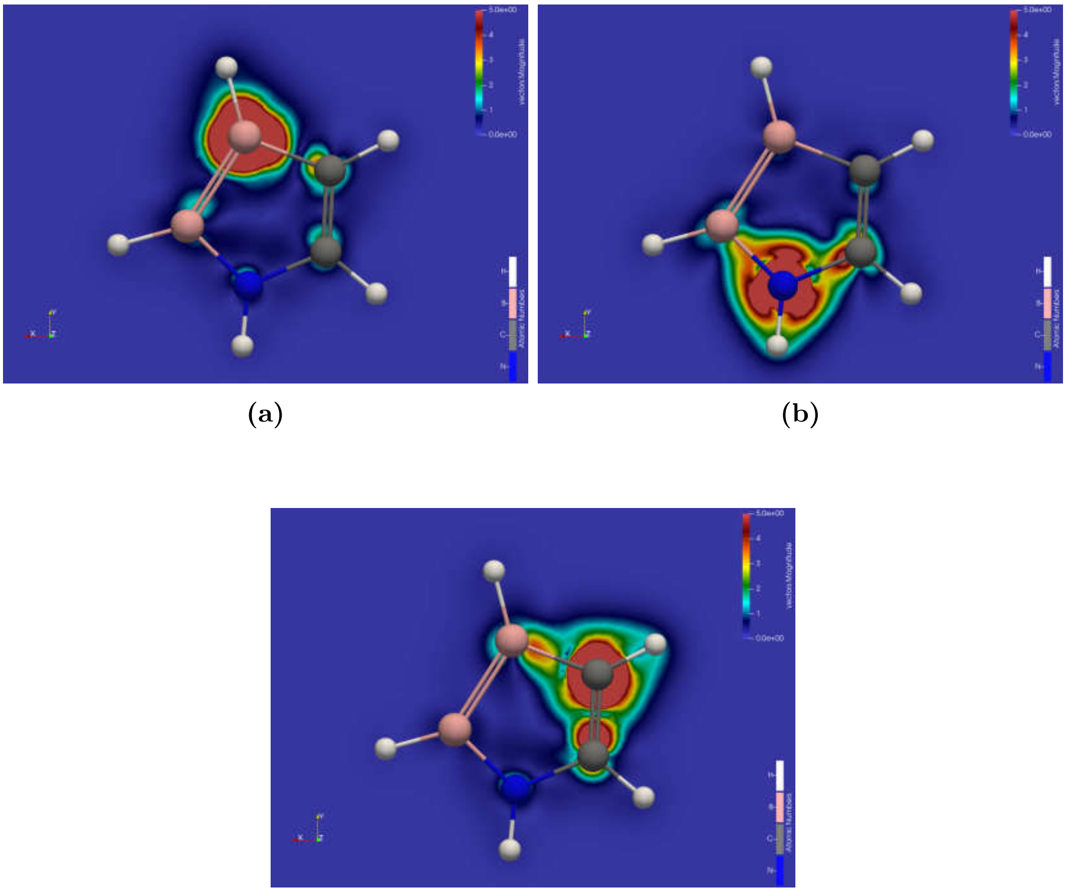
5.0e+00
4
3
2
1
0.0e+00
vectors Magnitude
H
B
C
N
Atomic Numbers
Y
X
Z

(a) **(b)**

(c)

Figure 5.5: Spatial contribution to the isotropic magnetic shielding of points in space for (a) boron (b) nitrogen (c) carbon of NBBCC

Chapter 6

Results and discussion

Benzene, cyclobutadiene and cyclopentadienyl anion

Benzene is the most studied aromatic molecule and is used here as a test molecule. For molecular structure calculations of benzene, we used two different basis sets: triple-ζ valence basis sets augmented by polarization functions (TZVP), and a quadruple-ζ valance basis sets augmented by polarization functions (QZVP) [33–35] . The NMR shielding constants are calculated using the module mpshift for TURBOMOLE [36]. The calculations with def2-QZVP using the B3LYP [34] functional with m3 grid gives a shielding constant of 46.81 for carbon and 23.73 for hydrogen, while for the basis set def2-TZVP using the B3LYP functional with m5 grid, we obtain a shielding constant of 51.11 and 23.95 for carbon and hydrogen respectively. TURBOMOLE calculates the shielding constants analytically as the second derivative of the energy, whereas GIMIC uses the numerical integration method, which might be inaccurate due to which the GIMIC methods leads to slightly different values from the TURBOMOLE reference data.

Table 6.1: *The isotropic magnetic shielding constants of C and H of benzene as obtained by* GIMIC *and* TURBOMOLE

Atom	GIMIC	TURBOMOLE
C	51.11285	51.11291
H	23.95653	23.95651

For the remaining calculations, a cuboidal grid was used as the number of points can be adjusted easily in them by increasing or decreasing the spacing between neighboring points. On increasing the number of grid points, the rationalization into paratropic and diatropic contribution to the magnetic shielding increases. The values of paratropic and diatropic shielding for different grid spacing for the carbon in benzene are as follows:

Table 6.2: *Paratropic and diatropic contributions to the shielding constant*

(a) *grid spacing of 0.25 a_0*

Atom	**Diatropic contribution to shielding**	**Paratropic contribution to shielding**
C	52.774	-1.673
C	51.560	-0.458
C	46.846	4.005
C	46.373	4.555
C	36.750	14.369
C	38.099	12.841

(b) *grid spacing of 0.15 a_0*

Atom	**Diatropic contribution to shielding**	**Paratropic contribution to shielding**
C	58.046	-6.944
C	54.414	-3.313
C	56.520	-5.419
C	54.224	-3.123
C	55.085	-3.985
C	57.009	-5.909

As we reduce the spacing, the values get closer and closer to the values obtained by TURBOMOLE, and the paratropic and diatopic contribution to the shielding constant converge respectively. As we change the spacing from 0.05 to 0.03 a_0, the values do not change much, and the final values are:

Table 6.3: *Contributions to the shielding constant with a grid spacing of 0.03 a_0*

(a) *Benzene*

Atom	**Diatropic contribution to shielding**	**Paratropic contribution to shielding**
C	60.209	-9.110
C	60.257	-9.158
C	60.281	-9.182
C	59.873	-8.774
C	60.310	-9.212
C	60.235	-9.136

(b) *Cyclobutadiene*

Atom	**Diatropic contribution to shielding**	**Paratropic contribution to shielding**
C	-43.32	92.02
C	-43.58	92.52
C	-43.13	91.75
C	-42.22	91.07

Benzene is the classic example of an aromatic molecule [37–39]. The criteria often used for aromaticity are low reactivity, planar structure, downfield proton chemical shifts, and magnetic susceptibility anisotropy. The reason for the large magnetic susceptibility anisotropy is the strong ring current in the molecular frame induced by the external magnetic field. The GIMIC calculations show that benzene has a strong diatropic ring current around the molecular ring and a weaker paratropic ring current inside the ring [40, 41].

Cyclobutadiene is an anti-aromatic [42, 43] molecule which, according to the ring-current model [2], sustains a net paratropic ring current. The calculations show that it sustains a strong paratropic ring current, mainly inside the molecular ring and a weak diatropic ring current outside the ring. The accuracy of the calculations of the current strength in cyclobutadiene also exhibit the same trend that when the spacing is decreased, the values for paratropic and diatropic contributions to the shielding converge respectively. Plots of the profile of the ring current through different integration planes are presented in Fig. 6.1 and Fig. 6.2.

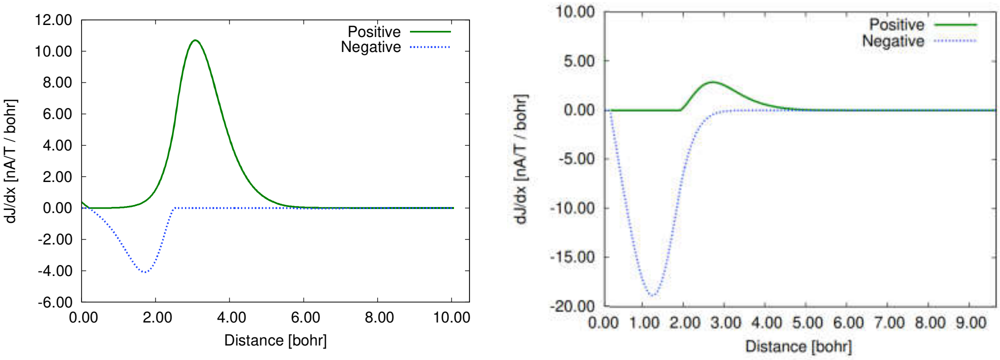

(a) Benzene

(b) Cyclobutadiene

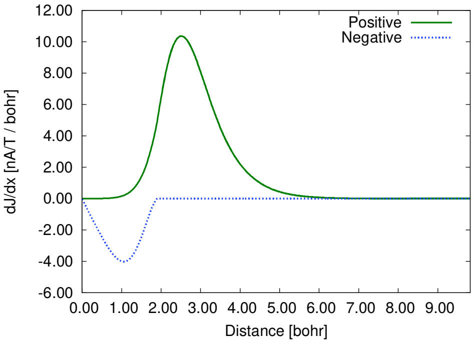

(c) Cyclopentadienyl anion

Figure 6.1: Strength of the ring currents in benzene, cyclobutadiene, and the cyclopentadienyl anion obtained by integrating through a C−C bond starting from the centre of the molecular ring to 8 a_0 away from the bond.

The integration of these plots or the area under the curve for both the positive and negative graphs give the diatropic and paratropic currents passing though that plane respectively.

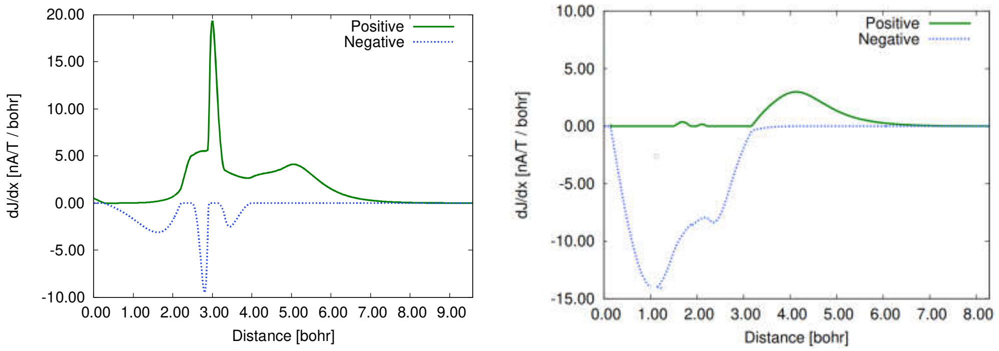

(a) Benzene **(b)** Cyclobutadiene

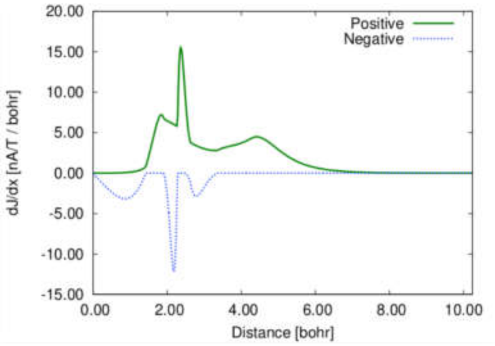

(c) Cyclopentadienyl anion

Figure 6.2: Strength of the ring currents in benzene, cyclobutadiene, and the cyclopentadienyl anion obtained by integrating through a C atom starting from the centre of the molecular ring to 8 a_0 away from the atom.

The current passing through benzene and cyclobutadiene are given in Table 6.4.

Table 6.4: *Current strengths (in nA T^{-1}) of the diatropic and paratropic contributions to the ring current of benzene and cyclobutadiene*

(a) *Benzene*

	Positive	**Negative**	**Total**
Atom	17.69	-6.14	11.54
Bond	16.47	-4.87	11.59

(b) *Cyclobutadiene*

	Positive	**Negative**	**Total**
Atom	-25.33	4.74	-20.58
Bond	-24.28	3.93	-20.34

The cyclopentadienyl anion is a five-membered planar ring with the chemical formula $C_5H_5{}^-$. It is an aromatic molecule as it contains 6π electrons and follows the Hückel rule of aromaticity [44–46]. The current density pathways and current strength plots show the presence of a weak paratropic current inside the ring with a strength -4.51 nA T^{-1}, which is surrounded by a strong diatropic current that extends outside the molecule making the molecule aromatic with a total strength of 17.42 nA T^{-1}. The overall current around the molecule is thus diatropic with a strength of 12.90 nA T^{-1} and hence the molecule is as aromatic as benzene.

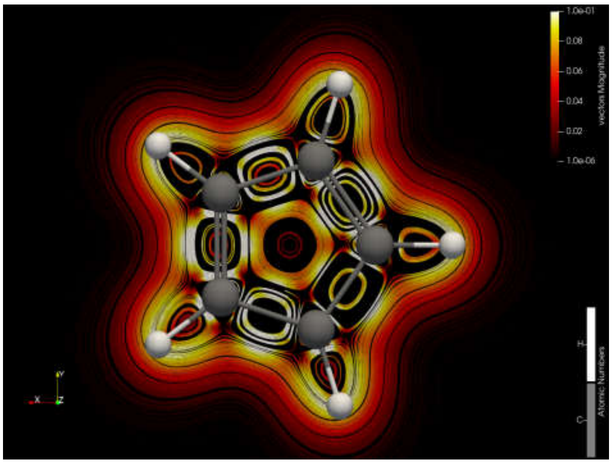
1.0e-01
0.08
0.06
0.04
0.02
1.0e-06
vectors Magnitude
H
C
Atomic Numbers
Y
X
Z

Figure 6.3: Magnitude of current density in the cyclopentadienyl anion

Naphthalene

Naphthalene consists of two six-membered rings fused by a common bond which leads to the formation of some interesting current-density pathways.

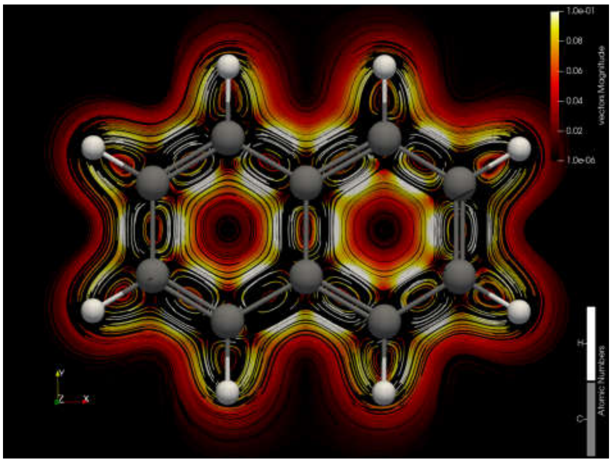
1.0e-01
0.08
0.06
0.04
0.02
1.0e-06
vectors Magnitude
H
C
Atomic Numbers
Y
Z
X

Figure 6.4: Magnitude of current density in naphthalene

As naphthalene is just two benzene rings fused, its current density pathway looks similar to the benzene current pathways, which can be seen in the current density pathways for naphthalene. It contains a strong diatropic current with a strength of 17.79 nA T^{-1} along the ring with a weaker paratropic current -4.65 nA T^{-1} in the center of the two rings.

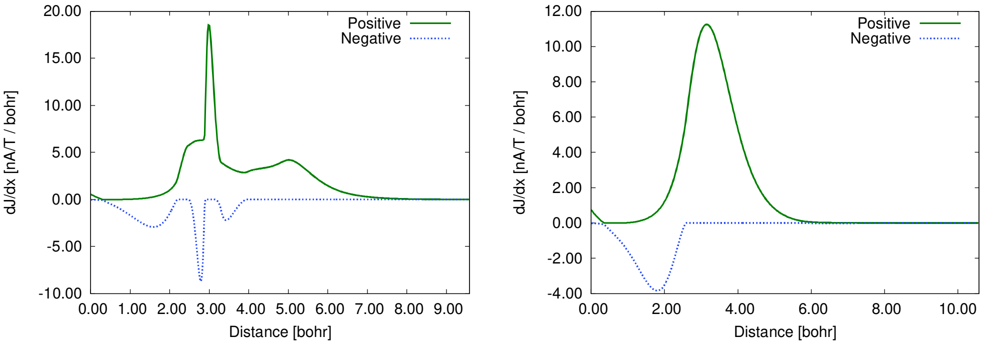

(a) **(b)**

Figure 6.5: Strength of the ring currents in napthalene obtained by integrating through a C−C bond and C atom starting from the centre of the molecular ring to 8 bohr away

Five-membered rings containing boron and nitrogen heteroatoms

We studied two isomers of a molecule with the chemical formula $C_2B_2NH_5$. The first molecule had the two boron adjacent to each other, and the two carbons also adjacent to each other attached to the boron via nitrogen (NB_2C_2) while the second molecule had both boron bonded to the nitrogen and one carbon while hydrogen atoms fulfilled the remaining valencies (NBC_2B).

Table 6.5: *Current strengths (in nA T^{-1}) for the five-membered rings with two boron atoms, two carbon atoms and one nitrogen atom obtained by integrating through a chemical bond.*

(a) *NBBCC*

	Positive	Negative	Total
Atom	-14.59	7.83	-6.76
Bond	-13.58	7.46	-6.11

(b) *NBCCB*

	Positive	Negative	Total
Atom	-12.39	7.64	-4.74
Bond	-13.64	9.19	-4.45

The current density pathways for the molecules are illustrated in Fig. 6.6. For both molecules, the current density around the nitrogen is quite strong and wrapped tightly around the atom with many weaker weak diatropic bond currents passing through the molecule. The current density inside the NBCCB molecule is strongly paratropic, which diminishes as we go away from the center of the molecule. The surrounding ring current around the perimeter of both molecules is a weaker diatropic current. The net current for the whole molecule is paratropic, which suggests that both molecules are anti-aromatic. The profiles of the current strength analysed from the centre of the five-membered ring through a C−C bond and reaching far from the molecule are presented in Fig. 6.7.

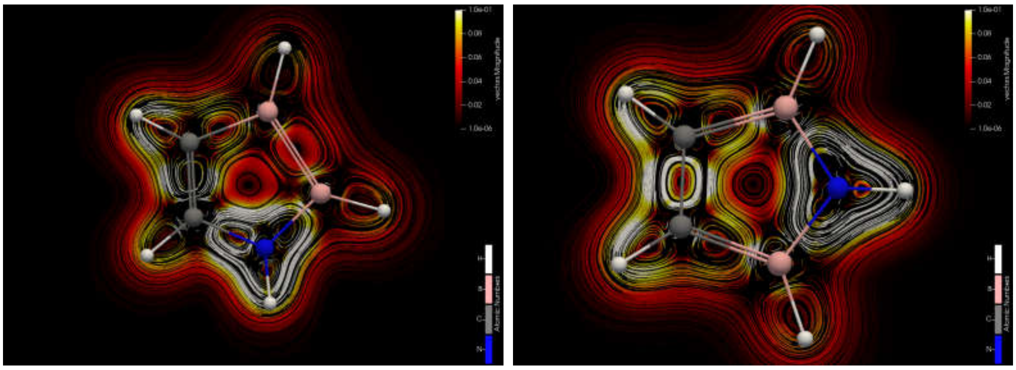

(a) **(b)**

Figure 6.6: Magnitude of the current densities in (a) NBBCC and (b) NB_2CBH_5 molecules

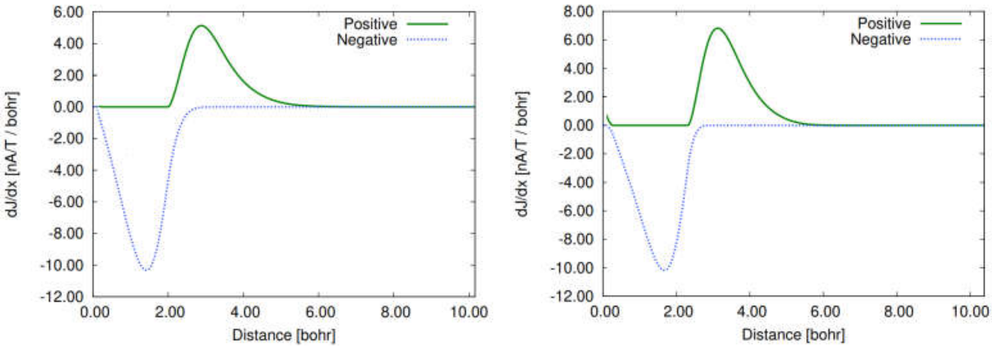

(a) **(b)**

Figure 6.7: Strength of currents in (a)NBBCC and (b) NBCCB molecules along the C−C bond

Caffeine

Caffeine is an interesting molecule as it contains two rings along with heteroatoms in both of the rings. The five-membered ring containing two nitrogen atoms while the six-member ring contains two nitrogen and two carbonyl carbons, which all have an interesting effect on the current density in the molecule.

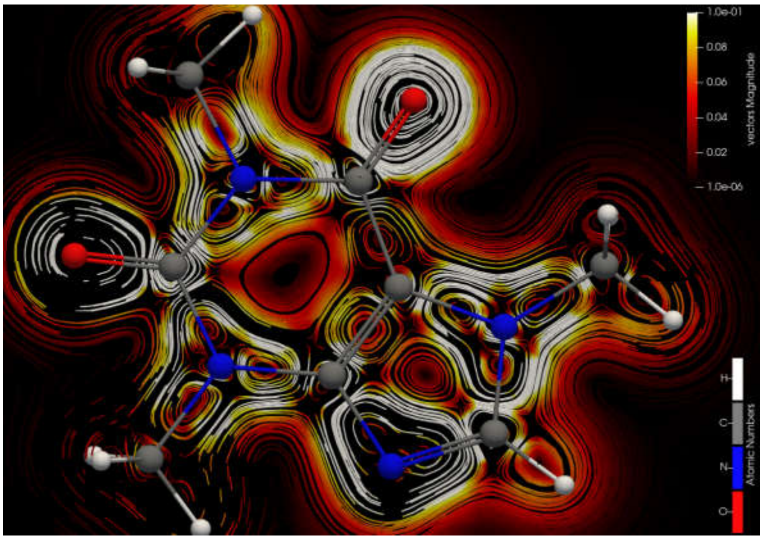

Figure 6.8: Magnitude of current density in caffeine

From the current density data, we can see that the six-membered ring contains a very weak diatropic current density, while the five-membered ring contains a stronger diatropic current density with a large current density surrounding the whole molecule. Current strength calculation on caffeine shows that the six-member ring contains a weak paratropic current of -6.66 nA T^{-1} inside the ring and an almost equally weak diatropic current of 7.44 nA T^{-1} along the ring. Due to this, the net current in the six-member ring is close to zero, making the ring non-aromatic. However, a weak diatropic current is present around the whole molecule with a strength of 6.16 nA T^{-1}. The five-membered ring sustains a stronger diatropic current of 12.88 nA T^{-1} making the ring aromatic, which is enveloped by the stronger molecule-wide current. The global molecular current for caffeine is 11.02 nA T^{-1} with the five-membered ring being aromatic while the 6 membered ring being non-aromatic.

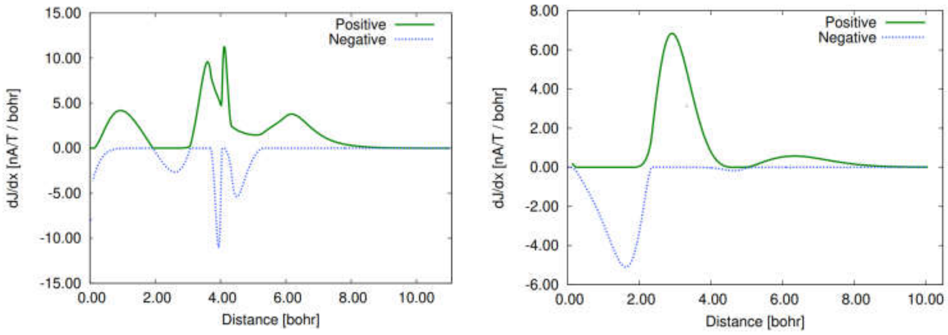

(a) **(b)**

Figure 6.9: Strength of currents in (a) five-membered ring (b) six-membered ring in caffeine

Methane, tetrafluoromethane and their trivalent anions

The shielding of carbon and fluorine in CF_4 and $CF_3{}^-$ are surprisingly different from each other as is reported in Ref. [47]. As the molecules are charged, the employed basis set is the valence triple-ζ with two sets of polarization functions and a set of diffuse functions (def2-TZVPPD) for the calculations on $CH_X{}^q$ and $CF_X{}^q$ (where $X = 4; 3$ and $q = 0; -1$ respectively). The DFT calculations were performed using the Minnesota 06 functional with 54% HF exchange (M06-2X) [48, 49] and the m5 grid. The isotropic shielding constants obtained with TURBOMOLE are listed in Table 6.6.

Table 6.6: *The calculated isotropic magnetic shielding constants of $CF_3{}^-$, $CH_3{}^-$, CF_4 and CH_4*

(a) $CX_3{}^-$

Atom	Isotropic
$C(CF_3{}^-)$	-3.66
$F(CF_3{}^-)$	200.08
$C(CH_3{}^-)$	230.22
$H(CH_3{}^-)$	34.59

(b) CX_4

Atom	Isotropic
$C(CF_4)$	57.41
$F(CF_4)$	242.86
$C(CH_4)$	194.02
$H(CH_4)$	31.80

Subsequently the GIMIC method was employed to calculate the diatropic and paratropic contributions to the shielding constants. The results are listed in Table 6.7.

Table 6.7: *The isotropic magnetic shielding decomposed into paratropic and diatropic contributions*

(a) $CX_3{}^-$

Atom	Paratropic	Diatropic
$C(CH_3{}^-)$	3.57	226.50
$H(CH_3{}^-)$	0.00025	34.56
$C(CF_3{}^-)$	-1.57	-2.17
$F(CF_3{}^-)$	0.69	200.52

(b) CX_4

Atom	Paratropic	Diatropic
$C(CH_4)$	-0.12	194.14
$H(CH_4)$	0.00014	31.79
$C(CF_4)$	-39.89	97.21
$F(CF_4)$	2.41	240.34

For CH_X, removing one hydrogen reduces the shielding by 40 ppm. As carbon is more electronegative than hydrogen, it withdraws electron density from hydrogen. On removing one hydrogen atom, the electron density on the carbon decreases, and hence the shielding of the nucleus is reduced. This can also be seen for the hydrogen atoms as their electron density also decreases and their shielding constants decrease because the carbon pulls more electron density when there is a lesser number of substituents bonded to it.

For CF_X, removing one fluorine has the opposite effect on the shielding compared to CH_X. The electron density on fluorine when there are only three fluorine atoms bonded

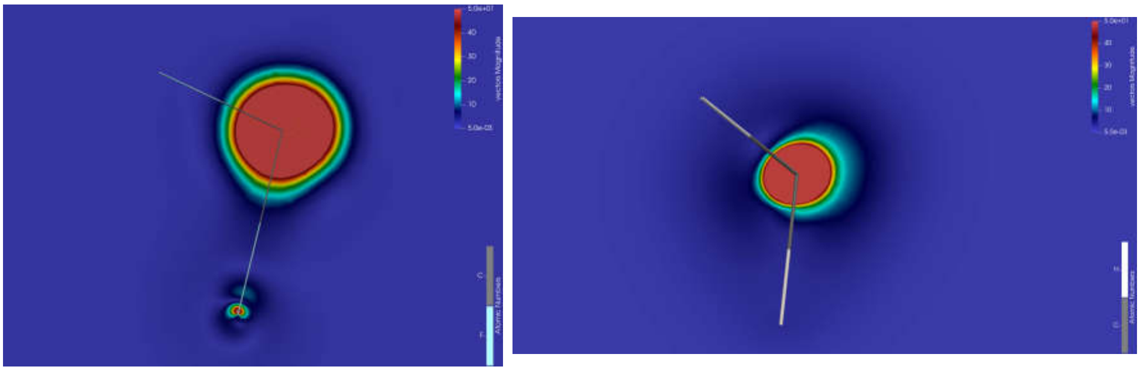

(a) **(b)**

Figure 6.10: Spatial contribution to the isotropic magnetic shielding constant of the carbon atom in (a) CF_3^- (b) CH_3^- along a C−X bond (X= F or H)

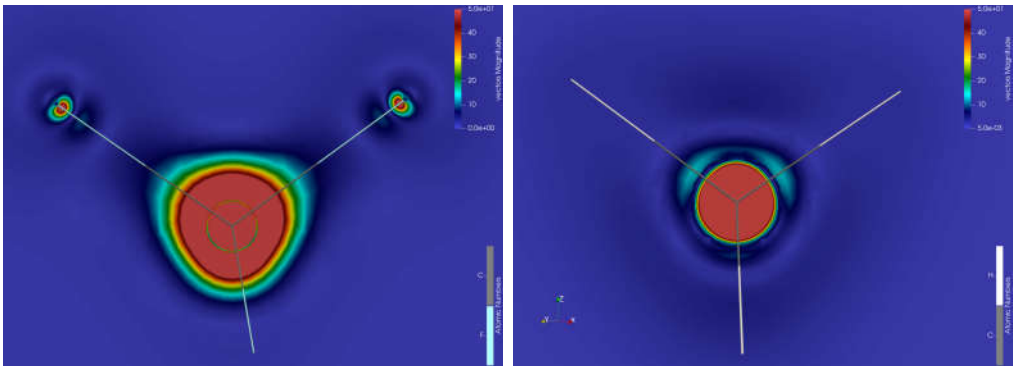

(a) **(b)**

Figure 6.11: Spatial contribution to the isotropic magnetic shielding constant for 'X' in (a) CF_4 (b) CH_4 along the X−C−X plane (X= F or H)

to the carbon is higher compared to the case when four fluorine atoms are present in the molecule. For carbon, however, this effect is not seen. From the isotropic contributions to the shielding, we can see that the paramagnetic contribution increases, however, the diatropic contribution decreases by about 100 ppm.

The shielding constant depends on the paratropic as well as the diatropic contributions to the nuclear shielding. This decomposition shows that the diatropic contribution to the shielding of the carbon lone pair is mainly responsible for the increase of this component in both the anions. However, similar decomposition for paratropic contribution is more complex as it involves the coupling of occupied and unoccupied orbitals [47]. The strength depends mainly on the strength of the magnetic coupling and energy gap between the coupled orbitals.

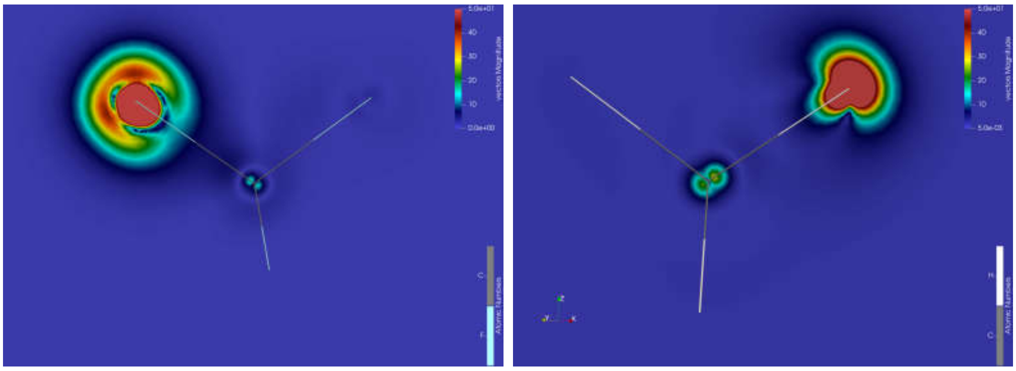

(a) **(b)**

Figure 6.12: Spatial contribution to the isotropic magnetic shielding constant of the carbon atom in (a) CF_4 (b) CH_4 along a X-C-X plane (X= F or H)

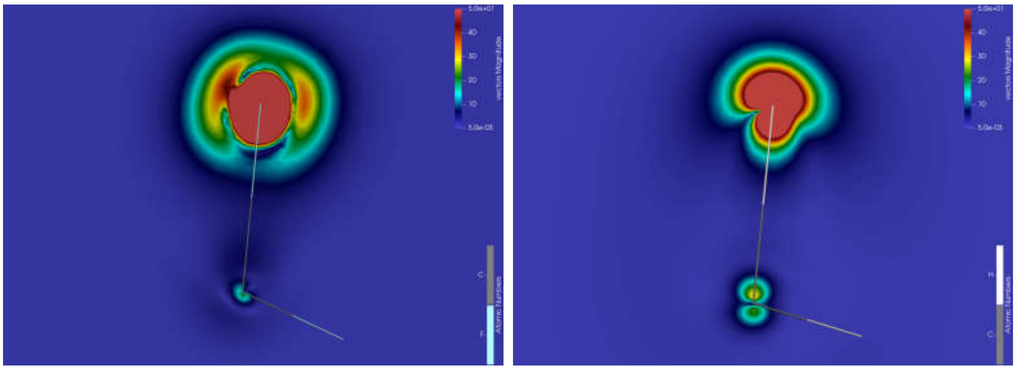

(a) **(b)**

Figure 6.13: Spatial contribution to the isotropic magnetic shielding constant for 'X' in (a) $CF_3{}^-$ (b) $CH_3{}^-$ along the C-X bond (X= F or H)

The overlap related to magnetic coupling is more substantial in $CF_3{}^-$ than in $CH_3{}^-$ due to dependency between the paratropic contribution and the electron nucleus distance. Although σ_{C-X} orbital contributions are essential to the total of σ_{para}, the lone pair contributions are essential to understand the unexpected de-shielding effect for the $CF_3{}^-$ molecule. When the carbanion is bonded to a fluorine atom, coupling between the lone pair of carbon and unoccupied sigma orbital is induced by the magnetic field producing a paramagnetic shielding on carbon.

Bibliography

[1] J. Jusélius, D. Sundholm, and co-workers, GIMIC, Gauge-Including Magnetically Induced Currents, a stand-alone program for the calculation of magnetically induced current density. `https://github.com/qmcurrents/gimic`.

[2] P. Lazzeretti., *Prog. Nucl. Magn. Reson. Spectrosc.* 36 (2000), 1–88.

[3] J. C. Facelli., *Prog. Nucl. Magn. Reson. Spectrosc.* 58 (2011), 176–201.

[4] W. H. Flygare., *The Journal of Chemical Physics* 41 (1964), 793–800.

[5] E. Schrödinger., *Ann. Phys. (Berlin)* 384 (1926), 489–527.

[6] E. Schrödinger., *Ann. Phys. (Berlin)* 385 (1926), 437–490.

[7] E. Schrödinger., *Ann. Phys. (Berlin)* 384 (1926), 361–376.

[8] E. Schrödinger., *Ann. Phys. (Berlin)* 386 (1926), 109–139.

[9] M. Born and J. R. Oppenheimer., *Ann. Physik* 84 (1927), 458.

[10] S. Gasiorowicz, *Quantum Physics*, Wiley, 1996.

[11] D. R. Hartree., *Math. Proc. Cambridge Philos. Soc.* 24 (1928), 89–110.

[12] D. R. Hartree., *Math. Proc. Cambridge Philos. Soc.* 24 (1928), 111–132.

[13] F. A. Bischoff and E. F. Valeev., *J. Chem. Phys.* 134 (2011), 104104.

[14] V. Fock., *Zeits. Phys.* 61 (1930), 126–148.

[15] R. McWeeny, *Methods of Molecular Quantum Mechanics*, Academic Press, 1992.

[16] J. Olsen, O. Christiansen, H. Koch, and P. Jørgensen., *J. Chem. Phys.* 105 (1996), 5082–5090.

[17] W. Kohn and L. J. Sham., *Phys. Rev.* 140 (1965), A1133–A1138.

[18] P. Hohenberg and W. Kohn., *Phys. Rev.* 136 (1964), B864–B871.

[19] A. D. Becke., *J. Chem. Phys.* 140 (2014), 18A301.

[20] A. D. Becke., *Phys. Rev. A* 33 (1986), 2786–2788.

[21] A. D. Becke., *J. Chem. Phys.* 84 (1986), 4524–4529.

[22] J. Tao, J. P. Perdew, V. N. Staroverov, and G. E. Scuseria., *Phys. Rev. Lett.* 91 (2003), 146401.

[23] J. P. Perdew, K. Burke, and M. Ernzerhof., *Phys. Rev. Lett.* 77 (1996), 3865–3868.

[24] K. Wolinski, J. F. Hilton, and P. Pulay., *J. Am. Chem. Soc.* 112 (1990), 8251–8260.

[25] D. Sundholm, H. Fliegl, and R. J. F. Berger., *WIREs Comput. Mol. Sci.* 6 (2016), 639–678.

[26] D. Sundholm, R. J. F. Berger, and H. Fliegl., *Phys. Chem. Chem. Phys.* 18 (2016), 15934–15942.

[27] N. F. Ramsey., *Phys. Rev.* 78 (1950), 699–703.

[28] J. Jusélius, D. Sundholm, and J. Gauss., *J. Chem. Phys.* 121 (2004), 3952–3963.

[29] S. T. Epstein., *J. Chem. Phys.* 58 (1973), 1592–1595.

[30] TURBOMOLE V7.4 2019, a development of University of Karlsruhe and Forschungszentrum Karlsruhe GmbH, 1989-2007, TURBOMOLE GmbH, since 2007, http://www.turbomole.com.

[31] J. C. Slater., *Phys. Rev.* 32 (1928), 339–348.

[32] E. Steiner and P. W. Fowler., *J. Phys. Chem. A* 105 (2001), 9553–9562.

[33] F. Jensen., *WIREs Comput. Mol. Sci.* 3 (2012), 273–295.

[34] F. Weigend and R. Ahlrichs., *Phys. Chem. Chem. Phys.* 7 (2005), 3297–3305.

[35] D. Feller and D. A. Dixon., *J. Phys. Chem. A* 122 (2018), 2598–2603.

[36] K. Reiter, F. Mack, and F. Weigend., *Journal of Chemical Theory and Computation* 14 (2018), PMID: 29232503, 191–197.

[37] T. M. Krygowski, M. K. Cyrañski, Z. Czarnocki, G. Häfelinger, and A. R. Katritzky., *Tetrahedron* 56 (2000), 1783–1796.

[38] T. M. Krygowski and M. K. Cyrański., *Chem. Rev.* 101 (2001), 1385–1420.

[39] Z. Chen, C. S. Wannere, C. Corminboeuf, R. Puchta, and P. v. R. Schleyer., *Chem. Rev.* 105 (2005), 3842–3888.

[40] J. A. N. F. Gomes., *Mol. Phys.* 47 (1982), 1227–1230.

[41] J. A. N. F. Gomes., *J. Chem. Phys.* 78 (1983), 4585–4591.

[42] R. Breslow., *Acc. Chem. Res.* 6 (1973), 393–398.

[43] P. R. von Schleyer and H. Jiao., *Pure Appl. Chem.* 68 (1996), 209–218.

[44] E. Hückel., *Zeits. Phys.* 70 (1931), 204–286.

[45] E. Hückel., *Zeits. Phys.* 72 (1931), 310–337.

[46] E. Hückel., *Zeits. Phys.* 76 (1932), 628–648.

[47] R. V. Viesser and C. F. Tormena., *Magn. Reson. Chem.* (2019).

[48] Y. Zhao and D. G. Truhlar., *Theor. Chem. Acc.* 120 (2007), 215–241.

[49] N. Mardirossian and M. Head-Gordon., *J. Chem. Theory Comput.* 12 (2016), 4303–4325.